ARTICLES

Room-temperature monoclinic distortion due to charge disproportionation in RNiO$_3$ perovskites with small rare-earth cations (R=Ho, Y, Er, Tm, Yb, and Lu): A neutron diffraction study

J. A. Alonso,* M. J. Martínez-Lope, and M. T. Casais
Instituto de Ciencia de Materiales de Madrid, C.S.I.C., Cantoblanco, E-28049 Madrid, Spain

J. L. García-Muñoz
Institut de Ciència de Materials de Barcelona, C.S.I.C., Campus UAB, Bellaterra, E-08193 Barcelona, Spain

M. T. Fernández-Díaz
Institut Laue-Langevin, B.P. 156, F-38042 Grenoble Cedex 9, France

(Received 4 August 1999)

Polycrystalline samples of the strongly distorted RNiO$_3$ (R=Ho, Y, Er, Tm, Yb, Lu) perovskites have been prepared under high hydrostatic pressure, at 20 kbar. The crystal structure in the insulating phase of these nickelates has been investigated by high-resolution neutron powder diffraction, below the metal-insulator (MI) transition that all of these compounds experience between 573 K (R=Ho) and 599 K (R=Lu). They present a subtle monoclinic distortion (s.g. $P2_1/n$) which implies the splitting of the Ni positions in the crystal. Ni1O$_6$ and Ni2O$_6$ octahedra exhibit very distinct mean Ni-O bond distances, interpreted as a charge disproportionation effect ($2\mathrm{Ni}^{3+} \rightarrow \mathrm{Ni}^{3+\delta} + \mathrm{Ni}^{3-\delta}$) which develops at the opening of the gap. In spite of the regular evolution of the β angle, characterizing the monoclinic distortion, the average $\langle$Ni1-O$\rangle$ and $\langle$Ni2-O$\rangle$ distances do not significantly change along the series; i.e., the disproportionation parameter δ is about 0.3 electrons in the last six members of the RNiO$_3$ series. The observed regular increase of the Ni1-O-Ni2 angles, governing the superexchange and the electronic transfer between Ni cations, accounts for the evolution of Néel and MI transition temperatures in these perovskites.

INTRODUCTION

RNiO$_3$ perovskites (R is a rare earth) have been extensively studied in the last few years[1] since the report of metal-to-insulator (MI) transitions as a function of temperature that systematically vary with the rare-earth size.[2,3] The occurrence of these thermally driven MI transitions has been related to the closing of the charge-transfer gap, induced by the narrowing of the electronic bandwidth when temperature decreases.[3,4] The degree of distortion of the structure determines the onset of electronic localization: for a given R^{3+} size the NiO$_6$ octahedra are tilted in order to optimize R-O bond distances, giving rise to bent Ni-O-Ni angles determining the degree of overlapping of Ni $3d$ and O $2p$ orbitals and, therefore, the electronic bandwidth. For the less-distorted rhombohedral LaNiO$_3$ perovskite, the degree of overlapping is enough to ensure metallic behavior;[5] for R^{3+} cations smaller than La^{3+} (R=Pr, Nd, Sm,...) the structure is orthorhombic and an abrupt change in the resistivity curves is observed at increasing temperatures: T_{MI} = 130 K (R=Pr), 200 K (R=Nd), 400 K (R=Sm), etc. Metal-like behavior is only observed above T_{MI}.

The observation of strong electron-lattice coupling in NdNiO$_3$ from infrared reflectivity measurements,[6] further confirmed in isotopically substituted RNiO$_3^{18}$ samples,[7] suggests the presence of polarons, associated with local charge fluctuations of the type Ni^{3+}-O^{2-} to Ni^{2+}-O^{1-}, which follow the movement of active e_g electrons. This picture could resemble that reported for LaMnO$_3$-related perovskites, in which the existence of magnetic polarons above T_C has been invoked to explain the colossal-magnetoresistance properties exhibited by these manganates.[8] In fact, Ni^{3+} is a Jahn-Teller (JT) ion ($t_{2g}^6 e_g^1$) as well as Mn^{3+} ($t_{2g}^3 e_g^1$), with a single e_g electron showing orbital degeneracy. In stoichiometric RMnO$_{3.00}$ oxides, static JT deformation breaks down the degeneracy, giving rise to significantly distorted MnO$_6$ octahedra.[9] In contrast, NiO$_6$ octahedra are almost regular in the first members of the RNiO$_3$ family, probably as a manifestation of the higher covalent character of Ni-O bonds.

This covalent character is expected to decrease along the series as R^{3+} cations become less electropositive. Therefore, it is of great interest the study of RNiO$_3$ perovskites for the smallest R^{3+} cations, in which the JT distortion and, thus, the electron-lattice interaction could be enhanced. Unhappily, the difficulties found in the preparation of these materials, inherent to the stabilization of Ni^{3+} cations, progressively increase along the series. In fact, all of the above-mentioned studies dealing with the crystal structure, MI transitions, and magnetic structure studies concern Pr, Nd, Sm, and Eu perovskites (or solid solutions among them):

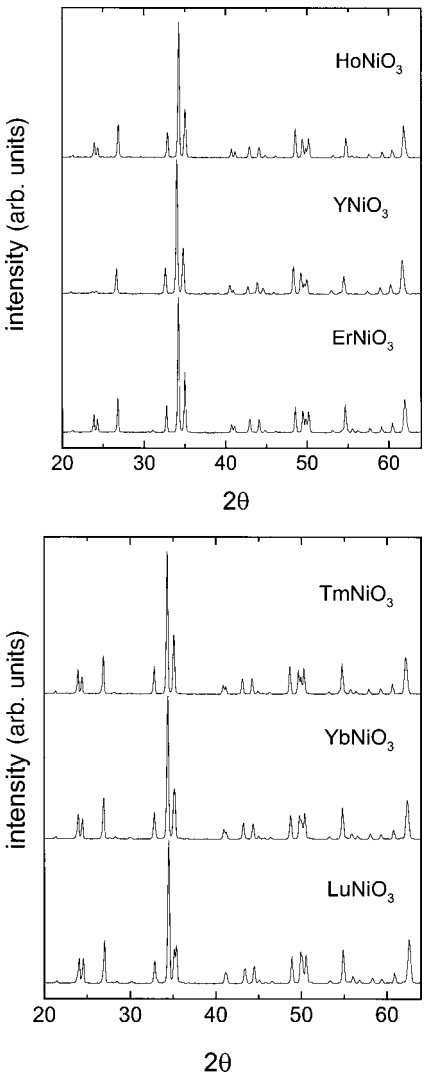

FIG. 1. XRD patterns for $R\mathrm{NiO_3}$.

these compounds can be obtained under moderate O_2 pressures (up to 200 bar). The remaining perovskites for R = Gd, Dy, Ho, Er, Yb, Lu, and Y had not been synthesized since the pioneering work by Demazeau *et al.*[10] in 1971. Very recently, we were able to prepare $YNiO_3$ and $HoNiO_3$ (Refs. 11 and 12) under hydrostatic pressure conditions, in sealed gold capsules in the presence of $KClO_4$ as an oxidizing agent. We described subtle structural changes associated to the MI transition of $YNiO_3$, at 582 K. In the metallic regime, above T_{MI}, the structure is orthorhombic (space group *Pbnm*), similar to that found for $Pr(Nd)NiO_3$,[4] but showing an increased distortion of the NiO_6 octahedra. The most striking finding, however, is the stabilization of a monoclinic structure (space group $P2_1/n$) in the insulating regime below T_{MI} for $HoNiO_3$ and $YNiO_3$ (Refs. 11 and 12); this structure is characterized by the existence of two alternating NiO_6 octahedra of different sizes, and reveals a charge disproportionation that develops at the opening of the charge-transfer gap. Further studies have shown that the monoclinic structure is also stable for the smallest R^{3+} cations, R = Er, Tm, Yb, and Lu, below their corresponding T_{MI}, in all cases above room temperature (RT).

High-resolution neutron powder diffraction (NPD) data, collected at room temperature in the insulating regime of $R\mathrm{NiO_3}$ (R = Y, Ho, Er, Tm, Yb, Lu) allowed us to fully characterize the crystal structure of the last members of this perovskite series. In this paper the structural parameters are reported, and their variation is discussed in the light of a bond-valence study.

EXPERIMENT

$R\mathrm{NiO_3}$ (R = Y, Ho, Er, Tm, Yb, Lu) perovskites were prepared as polycrystalline powders from stoichiometric mixtures of R_2O_3 and NiO. For each compound, the starting oxides were mixed and thoroughly ground with $KClO_4$ (30% in weight), put into a gold capsule (8-mm diameter, 10-mm length), sealed and placed in a cylindrical graphite heater. The reaction was carried out in a piston-cylinder press (Rockland Research Co.), at a pressure of 20 kbar at 900 °C for 20 min. Then the material was quenched to room temperature and the pressure was subsequently released. The product was ground and washed in a dilute HNO_3 aqueous solution, in order to dissolve KCl coming from the decomposition of $KClO_4$ and to eliminate small amounts of impurity phases (mainly unreacted oxides); the powder samples were finally dried in air at 150 °C for 1 h.

X-ray powder diffraction (XRD) patterns were collected for phase identification and to assess phase purity using Cu $K\alpha$ radiation in a Siemens D-501 goniometer controlled by a DACO-MP computer. The crystal structure of $R\mathrm{NiO_3}$ was studied by NPD at room temperature. In spite of the relatively small amount of sample available (800 mg), good quality patterns were collected at D2B high-resolution diffractometer at ILL-Grenoble. The wavelength used was 1.594 Å, and the counting time 8 h in the high-flux mode. The Rietveld program FULLPROF (Ref. 13) was used to analyze the data. Since small amounts of NiO or R_2O_3 were identified in Er and Yb patterns, the impurities were introduced as a second phase in the final refinement.

RESULTS

$R\mathrm{NiO_3}$ (R = Y, Ho, Er, Tm, Yb, Lu) samples were obtained as black, well-crystallized powders. The laboratory XRD diagrams are shown in Fig. 1. The patterns are characteristic of strongly distorted perovskites showing sharp, well-defined superstructure reflections. The structural refinement was performed from NPD data in the monoclinic $P2_1/n$ space group, with unit-cell parameters related to $\mathbf{a}_0$ (ideal cubic perovskite, $\mathbf{a}_0 \approx 3.8$ Å) as $\mathbf{a} \approx \sqrt{2}\mathbf{a}_0$, $\mathbf{b} \approx \sqrt{2}\mathbf{a}_0$, and $\mathbf{c} \approx 2a_0$, using as starting model the already reported structure for $YNiO_3$.[11] In $P2_1/n$ there are two crystallographically independent Ni positions (Ni1 and Ni2), as well as three kinds of nonequivalent oxygen atoms (O1, O2, and O3) all in general (x,y,z) positions. The final atomic coordinates, unit-cell parameters, and agreement factors from the refinements are given in Table I. The monoclinic β angle is, in all cases, smaller than 90.17°: the metric of this structure seems to be strongly pseudo-orthorhombic. Figure 2 shows the agreement between observed and calculated NPD profiles for the most distorted $LuNiO_3$ perovskite. Table II contains selected bond distances and angles. The crystal structure is illustrated in Fig. 3 for $LuNiO_3$. The NiO_6 octahedra are fairly tilted

TABLE I. Unit-cell, positional, and thermal parameters for RNiO$_3$ in the monoclinic $P2_1/n$ space group, $Z=4$, from NPD data at 295 K. Reliability factors for both patterns are also given. For R=Ho and Y synchrotron XRD data are combined with NPD data (from Refs. 11 and 12).

R	Ho	Y	Er	Tm	Yb	Lu
a (Å)	5.182 00(4)	5.179 32(5)	5.1614(1)	5.1453(1)	5.1298(1)	5.1109(1)
b (Å)	5.510 50(4)	5.515 29(5)	5.5110(1)	5.5038(1)	5.4996(1)	5.4984(1)
c (Å)	7.423 36(5)	7.416 56(7)	7.3997(1)	7.3750(1)	7.3404(1)	7.3404(1)
β (°)	90.084(1)	90.081(1)	90.112(1)	90.115(1)	90.125(1)	90.163(1)
V (Å^3)	211.977(4)	211.857(5)	210.48(1)	208.85(1)	207.46(1)	206.28(1)
R $4e(x\ y\ z)$						
x	0.981 81(9)	0.9816(2)	0.9809(3)	0.9797(5)	0.9796(2)	0.9766(4)
y	0.071 77(7)	0.0729(1)	0.0733(2)	0.007 54(2)	0.0764(1)	0.0779(2)
z	0.2503(2)	0.2502(4)	0.2504(5)	0.2503(7)	0.2496(3)	0.2509(4)
$10^2B_{\rm iso}$ (Å^2)	0.47(1)	0.52(2)	0.27(2)	0.27(3)	0.30(2)	0.31(3)
Ni1 $2d$ ($\frac{1}{2}$ 0 0)						
$10^2B_{\rm iso}$ (Å^2)	0.36(7)	0.55(5)	0.40(4)	0.28(5)	0.27(4)	0.30(4)
Ni2 $2c$($\frac{1}{2}$ 0 $\frac{1}{2}$)						
$10^2B_{\rm iso}$ (Å^2)	0.34(7)	0.28(5)	0.38(5)	0.20(5)	0.26(4)	0.29(4)
O1 $4e(x\ y\ z)$						
x	0.0983(6)	0.0998(3)	0.1019(3)	0.1046(5)	0.1074(4)	0.1121(4)
y	0.4700(6)	0.4705(3)	0.4694(3)	0.4666(4)	0.4637(3)	0.4633(4)
z	0.2447(9)	0.2457(5)	0.2456(4)	0.2448(5)	0.2453(4)	0.2443(4)
$10^2B_{\rm iso}$ (Å^2)	0.63(7)	0.54(4)	0.33(3)	0.30(4)	0.35(3)	0.42(4)
O2 $4e(x\ y\ z)$						
x	0.700(1)	0.6973(7)	0.6990(6)	0.6996(7)	0.6950(5)	0.6949(5)
y	0.310(1)	0.3080(7)	0.3088(6)	0.3106(8)	0.3123(6)	0.3112(6)
z	0.0494(7)	0.0467(5)	0.0505(4)	0.0505(5)	0.0524(4)	0.0539(4)
$10^2B_{\rm iso}$ (Å^2)	0.50(12)	0.55(6)	0.51(4)	0.40(6)	0.39(4)	0.41(4)
O3 $4e(x\ y\ z)$						
x	0.187(1)	0.1882(6)	0.1852(5)	0.1833(6)	0.1827(5)	0.1824(5)
y	0.206(1)	0.2038(7)	0.2021(6)	0.2020(8)	0.2008(6)	0.2004(6)
z	0.9482(8)	0.9465(5)	0.9476(4)	0.9455(5)	0.9446(4)	0.9446(4)
$10^2B_{\rm iso}$ (Å^2)	0.63(12)	0.57(7)	0.48(4)	0.27(5)	0.44(4)	0.47(4)
Reliability factors						
χ^2	1.679	1.691	1.60	1.21	1.50	1.49
Synchrotron data						
R_p	0.077	0.092				
R_{wp}	0.094	0.111				
R_I	0.026	0.050				
Neutron data						
R_p	0.044	0.035	0.025	0.034	0.031	0.037
R_{wp}	0.054	0.043	0.032	0.042	0.039	0.047
$R_{\rm exp}$			0.025	0.038	0.032	0.038
R_I	0.051	0.030	0.045	0.045	0.031	0.047

due to the small size of Lu^{3+} cations, in order to optimize the Lu-O bond distances. Ni1O$_6$ and Ni2O$_6$ octahedra are fully ordered, and alternate along the three directions of the crystal, in such a way that each Ni1O$_6$ octahedron is linked to six Ni2O$_6$ octahedra, as shown in Fig. 3, and vice versa.

The phenomenological Brown's bond valence model estimates the formal valence of a bond from the measured bond lengths in nonstrained structures (for each central atom, $v=\Sigma s_i$, $s_i=\exp[(r_0-r_i)/B]$).[14,15] The valences calculated by using this approach in the ionic limit are listed in Table III for all the atoms. The departure of the bond valence sum rule is a measure of the existing stress in the bonds of the structure. The overall stress can be quantified by means of a global instability index (GII),[16] calculated as the root mean of the valence deviations for the $j=1,\ldots,N$ atoms in the asymmetric unit; the GII is equal to $(\Sigma_j[\Sigma_i(s_{ij}$

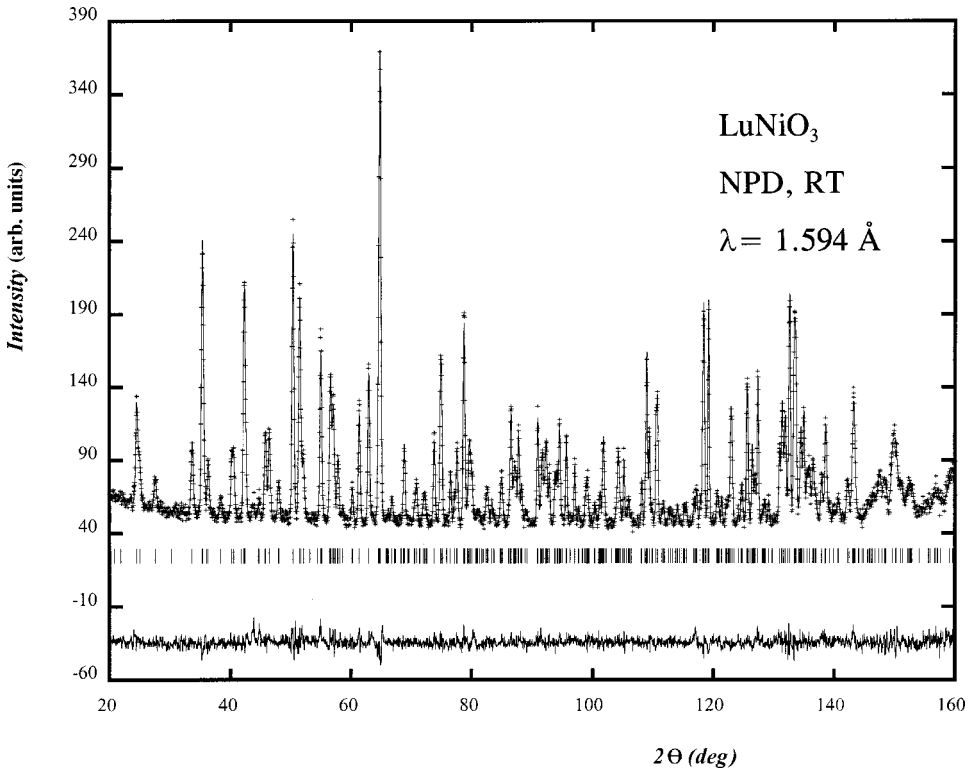

FIG. 2. Observed (crosses), calculated (full line), and difference (bottom) NPD Rietveld profiles for $LuNiO_3$ at 295 K.

$-V_j)^2]/N)^{1/2}$. GII values are also included in Table III. Valences significantly lower than +3 for Ni1 and higher than +3 for Ni2 are observed in all the compounds (Table III). Consequently, the appearance of two alternating Ni states with $3+\delta, 3-\delta'$ valences give evidence of a charge disproportionation phenomenum associated to the insulating phase of pure $R NiO_3$ perovskites.

DISCUSSION

It is worth emphasizing that the MI transition occurs well above room temperature in all the compounds investigated in the present work [between $T_{MI}=573$ K (R=Ho) and $T_{MI}=599$ K (R=Lu)].[17] Therefore, at RT the transition has come to completion in all the cases. That is, structural data gathered in Tables I and II were obtained from samples with a 100% of the insulating fraction at RT. Moreover, it is important to underline that the high-resolution NPD data could not be successfully refined in the conventional *Pbnm* orthorhombic symmetry. The perovskites with Ho, Y, Er, Tm, Yb, and Lu (decreasing in R^{3+} size) are all found to be monoclinic. The diffraction patterns are well reproduced using the $P2_1/n$ space group, previously reported for Y and Ho compounds.[11,12] This finding confirms that the lowering of crystallographic symmetry in $R NiO_3$ perovskites with small (and perhaps not so small) rare-earth cations is a common feature across the MI transition.

Figure 4(a) illustrates the monotonous evolution of unit-cell parameters with the size of the rare-earth cation. Figure 4(b) shows the linear evolution of the monoclinic cell volume. Whereas in the metallic state $dV(\mathrm{RT})/dR_0=104$ Å^2,[18] we have found $dV(\mathrm{RT})/dR_0=152$ Å^2 in the present monoclinic compounds. Ni1 and Ni2 sites are arranged like a checkerboard within the *ab* plane, alternating as well along the *c* axis. The monoclinic distortion presents identical qualitative features in all the compounds. The mean Ni-O distance in the $Ni1O_6$ octahedron [2.000(3) Å] is larger than in the $Ni2O_6$ [1.915(3) Å]. The distortion of the NiO_6 octahedra is comparable for Ni1 and Ni2 sites (somewhat smaller in Ni2 octahedra). The distortion parameters Δ_d given in Table II fall within the interval $0.8–1.6\times10^{-4}$. On the one hand, this static distortion is one order of magnitude larger than in the insulating phase with Sm ($\Delta_d\approx1.6\times10^{-5}$)[19] and two orders larger than with Pr ($\Delta_d\approx1.4\times10^{-6}$).[4] This is indicative of a systematic increase of the deformation going to smaller rare-earth cations. On the other hand the deformation is very small compared to the expected value for a JT distorted octahedra. In particular, it is around 30 times smaller than the deformation found in $LaMnO_3$ ($\Delta_d\approx3.3\times10^{-3}$).[9]

These features observed for the nickelates with small rare-earth cations are in sharp contrast with the charge-ordering phenomena observed in many $R_{1/2}Ca_{1/2}MnO_3$ oxides: for instance, in the charge-ordered state of $R_{1/2}Ca_{1/2}MnO_3$ identical planes of alternating Mn^{3+} and Mn^{4+} sites are stacked along the *c* axis.[20] One of the e_g orbitals is occupied at alternating sites in the planes, in such a way that there are rods of Mn^{3+} (d^4) octahedra parallel to the *c* axis with all $3y^2-r^2$ (or all $3x^2-r^2$) occupied. These octahedra are accompanied by a strong JT distortion. Moreover, this particular orbital ordering is favored by the fact that the eight oxygen atoms nearest to the *R*-site ion shift practically in the same direction, favoring the *R*-O hybridization. In the case of the monoclinic nickelates investigated in this work, there is no doubt that the observed crystal structure and the concomitant charge disproportionation are not favoring a possible JT distortion associated with the e_g electron of Ni^{3+} cations (d^7). From examination of data in Tables II and III, there are no indications of orbital ordering in these materials.

An essential point of this study is the evolution of the

TABLE II. Main bond distances (Å) and selected angles (°) for monoclinic RNiO$_3$, determined from NPD data at 295 K. The distortion parameter Δd for NiO$_6$ octahedra with an average Ni-O distance $\langle d\rangle$ is defined as $\Delta_d=(\frac{1}{6})\Sigma_{n=1,6}[(d_n-\langle d\rangle)/\langle d\rangle]^2$.

R	Ho	Y	Er	Tm	Yb	Lu
Ni1O$_6$ octahedra						
Ni1-O1 (×2)	1.970(6)	0.963(4)	1.963(3)	1.967(4)	1.964(3)	1.975(3)
Ni1-O2 (×2)	2.031(6)	2.012(4)	2.022(3)	2.028(4)	2.024(3)	2.019(3)
Ni1-O3 (×2)	2.015(6)	2.006(3)	2.007(3)	2.013(4)	2.008(3)	2.003(3)
⟨Ni-O⟩	2.005(6)	1.994(4)	1.997(3)	2.003(4)	1.999(3)	1.999(3)
$10^4\Delta_d$	1.66	1.20	2.66	1.68	1.61	0.83
Ni2O$_6$ octahedra						
Ni2-O1 (×2)	1.893(6)	1.901(4)	1.898(3)	1.892(4)	1.895(3)	1.892(3)
Ni2-O2 (×2)	1.911(6)	1.924(3)	1.915(3)	1.902(4)	1.914(2)	1.915(3)
Ni2-O3 (×2)	1.927(7)	1.944(4)	1.939(3)	1.934(4)	1.938(3)	1.937(3)
⟨Ni2-O⟩	1.910(6)	1.923(4)	1.917(3)	1.909(4)	1.916(3)	1.915(3)
$10^4\Delta_d$	0.53	0.83	0.77	0.88	0.84	0.92
⟨Ni-O⟩	1.958(6)	1.959(4)	1.957(3)	1.956(4)	1.958(3)	1.957(3)
Ni1-O1-Ni2 (×2)	147.8(2)	147.4(1)	146.8(1)	145.7(1)	144.6(1)	143.4(1)
Ni1-O2-Ni2 (×2)	147.2(3)	147.9(2)	147.1(1)	146.8(1)	145.4(1)	145.1(1)
Ni1-O2-Ni2 (×2)	147.2(4)	146.5(2)	146.2(1)	145.3(1)	144.8(1)	144.6(1)
RO$_9$ polyhedra						
R-O1	2.276(3)	2.277(2)	2.271(2)	2.247(3)	2.229(2)	2.230(3)
R-O1[a]	3.058(3)	3.064(2)	3.062(2)	3.066(3)	3.075(2)	3.074(3)
R-O1	2.247(3)	2.241(2)	2.229(2)	2.222(3)	2.208(2)	2.195(3)
R-O2	2.466(6)	2.474(4)	2.446(4)	2.432(5)	2.431(3)	2.408(4)
R-O2	2.276(6)	2.295(4)	2.273(4)	2.267(5)	2.245(3)	2.232(4)
R-O2	2.573(6)	2.552(4)	2.571(4)	2.563(6)	2.558(3)	2.560(4)
R-O3	2.592(6)	2.597(4)	2.577(4)	2.578(6)	2.568(3)	2.575(4)
R-O3	2.298(7)	2.286(4)	2.449(4)	2.430(5)	2.426(3)	2.405(4)
R-O3	2.448(6)	2.440(4)	2.277(4)	2.262(5)	2.248(3)	2.247(4)
$\langle R\text{-O}\rangle_{8\ \mathrm{short}}$	2.397(4)	2.395(3)	2.386(3)	2.375(4)	2.364(2)	2.356(3)
⟨R-O⟩	2.470(4)	2.470(3)	2.462(3)	2.452(4)	2.443(2)	2.436(3)

[a]Long R-O distances.

charge-disproportionation degree along the series. The redistribution of charges can be understood as a mutual self-doping process occurring at T_{MI}, in which a fraction of negative charge leaves the Ni2 octahedra and goes to neighboring Ni1 sites.[12] Hence the difference between the two Ni-O distances is very akin to the degree of disproportionation (δ) in $2\mathrm{Ni}^{3+}\leftrightarrow\mathrm{Ni}^{3+\delta}+\mathrm{Ni}^{3-\delta'}$. In Fig. 5(a) we depict the values given in Table II for the ⟨Ni1-O⟩ and ⟨Ni2-O⟩ bond lengths obtained at RT. It is important to note that our data do not give indications of systematic changes in the size difference between Ni1O$_6$ and Ni2O$_6$ octahedra on going from Ho to Lu. On the contrary, mean ⟨Ni1-O⟩ and ⟨Ni2-O⟩ bond lengths are found to remain unchanged in the six monoclinic samples. In order to monitor the degree of disproportionation one can define the effective charge variation $\delta_{\mathrm{eff}}=(\delta+\delta')/2$. The calculated valences (ionic limit) are practically identical in all the cases: the mean values are 2.58(2) and 3.24(2), respectively, for Ni1 and Ni2 cations (see also Refs. 11 and 12), giving $\delta_{\mathrm{eff}}=0.33(2)$. Taking into consideration the dispersion of points in Fig. 5(a) as well as the estimated errors, an upper limit can be given for possible small changes in the disproportion degree along the series. The corresponding estimation implies that the valence change in Ni1 and Ni2 along the series, if any, should be smaller than 2% with respect to the mean 2.58(2) and 3.24(2) values. We are thus led to conclude that in all of these oxides Ni1 octahedra contains in the insulating state around ~0.6 electrons more than Ni2 octahedra.

The evolution of the exchange interactions in RNiO$_3$ perovskites is controlled by the superexchange angle θ = Ni-O-Ni. In Fig. 6(a) we plot the average Ni-O-Ni angle against R_0. The angular variation of the mean Ni-O overlap $[\approx(1-\cos(\pi-\theta/4))]$ varies ≈16% form Ho to Lu. As expected, this variation is very similar to the change observed in T_N (14%) for the two extreme samples (146 and 128 K; respectively, for Ho and Lu). By contrast, in mixed valence magnetoresistive manganites, the variation of the ferromagnetic T_C with R_0 is too large to be explained by the angular variation $\theta(R_0)$. As a result, covalent mixing effects[21,22] have been invoked to explain the changes in the covalence of Mn-O bonds with R_0. They are based on the competition between the electronegativity of A- and B-site cations, both bonded to the same O:2p anions. In our case, the constant ⟨Ni-O⟩ bond length suggests that this effect does not play a significant role in the late members of the RNiO$_3$ series. In Fig. 5(b) the mean ⟨R-O⟩ distance behaves linearly with slope 1.

Finally, we shall focus on the evolution of the monoclinic

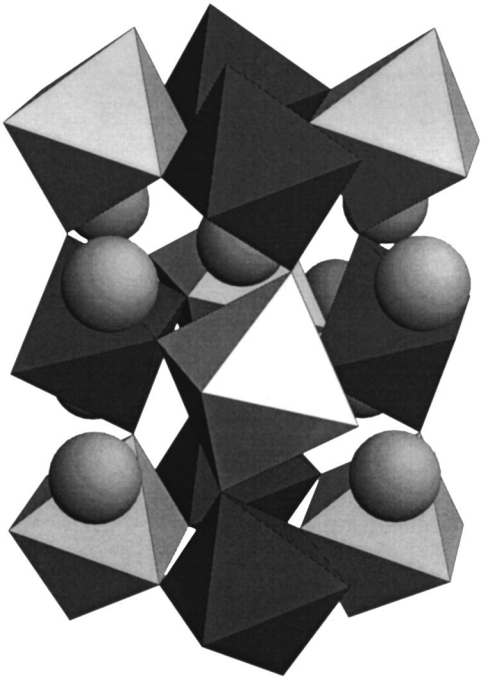

FIG. 3. View of the structure of monoclinic $LuNiO_3$. The **c** axis is vertical, and the **a** axis goes from right to left. Large spheres represent Lu; corner-sharing $Ni1O_6$ (dark) and $Ni2O_6$ octahedra are fairly tilted in the structure to optimize Lu-O bond lengths.

distortion, which is one of the main findings of the present work. The refinements in the monoclinic model give a perfect account of the splitting observed in some reflections, which is directly akin to a deviation of the β angle from 90°. In all of the investigated samples this deviation is very small but the high-resolution NPD data allowed us to determine its evolution with very good accuracy. The corresponding values are given in Table I, and are also represented against R_0 in Fig. 6(b). It is found that the monoclinic angle systematically increases when reducing the size of the A cation. Although the deviation from 90° is always small, the variation

TABLE III. Valences determined from the bond valence model for R, Ni, and O within the RO_8 and NiO_6 coordination polyhedra in $RNiO_3$. The valence is the sum of the individual bond valences (s_i) for R-O and Ni-O bonds. Bond valences are calculated as $s_i = \exp[(r_0 - r_i)B]$; $B = 0.37$; and $r_0 = 1.686$ for the Ni^{3+}-O^2 pair; for the R^{3+}-O^{2-} pairs, from Ho, Y . . . to Lu, $r_0 = 2.023$, 2.014, 2.010, 2.000, 1.985, and 1.971, from Ref. 15. Individual R-O and Ni-O distances (r_i) are taken from Table II. The global instability index (GII) is calculated as the root mean of the valence deviations for the $j = 1, \ldots, N$ atoms in the asymmetric unit, and is equal to $(\Sigma_j[\Sigma_i(s_{ij} - V_j)^2]/N)^{1/2}$.

R	Ho	Y	Er	Tm	Yb	Lu
R	3.09(2)	3.03(1)	3.07(1)	3.09(1)	3.08(1)	3.03(1)
Ni1	2.53(2)	2.62(1)	2.59(1)	2.56(1)	2.58(1)	2.58(1)
Ni2	3.28(2)	3.17(1)	3.22(1)	3.28(1)	3.23(1)	3.24(1)
O1	2.09(1)	2.07(1)	2.09(1)	2.10(1)	2.11(1)	2.08(1)
O2	1.97(1)	1.93(1)	1.96(1)	1.97(1)	1.95(1)	1.95(1)
O3	1.94(1)	1.92(1)	1.93(1)	1.94(1)	1.93(1)	1.91(1)
GII	0.229	0.179	0.197	0.244	0.204	0.204

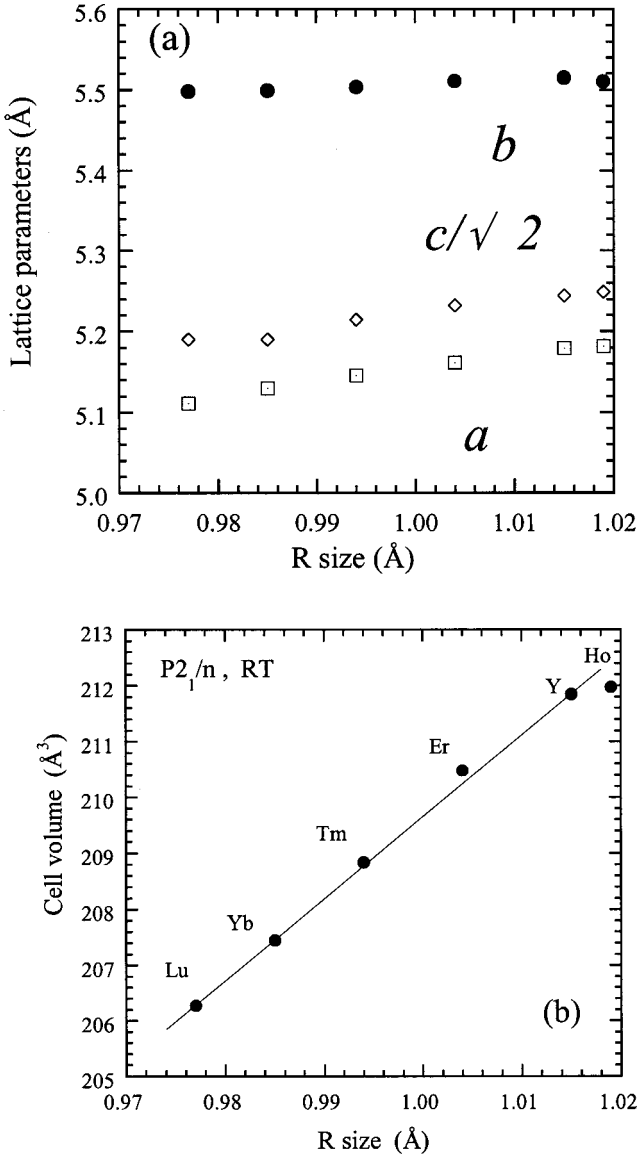

FIG. 4. (a) Unit-cell parameters and (b) volume variation with the size of the rare-earth cation.

is very significant when compared to the estimated errors. Several remarks may be done in the light of the evolution shown in Fig. 6(b). (i) First, an extrapolation of the β values to less distorted perovskites cuts the 90° line near the R_0 value that corresponds to the Eu sample. (ii) Second, if the deviation from 90° of the β angle is used to quantify the degree of monoclinic distortion, Fig. 6(b) reveals that the degree of monoclinic distortion is not related with the observed Ni1 and Ni2 valences, i.e., with the value of δ_{eff}. For the same degree of charge disproportionation we find a continuous variation of the monoclinic angle. This is equivalent to say that there is not a direct relationship between the parameters δ_{eff} and β. This is of great importance if one considers the possible charge disproportionation in larger rare-earth nickelates. The perovskites with $R = \text{Pr}, \ldots, \text{Dy}$ do not show any detectable splitting of the diffraction peaks that justify the lowering of crystal symmetry below the MI transition.[12,23] Instead, the strain inherent to the distortion is releaved through structural mistakes such as stacking faults and intergrowths, giving rise to the observation of aniso-

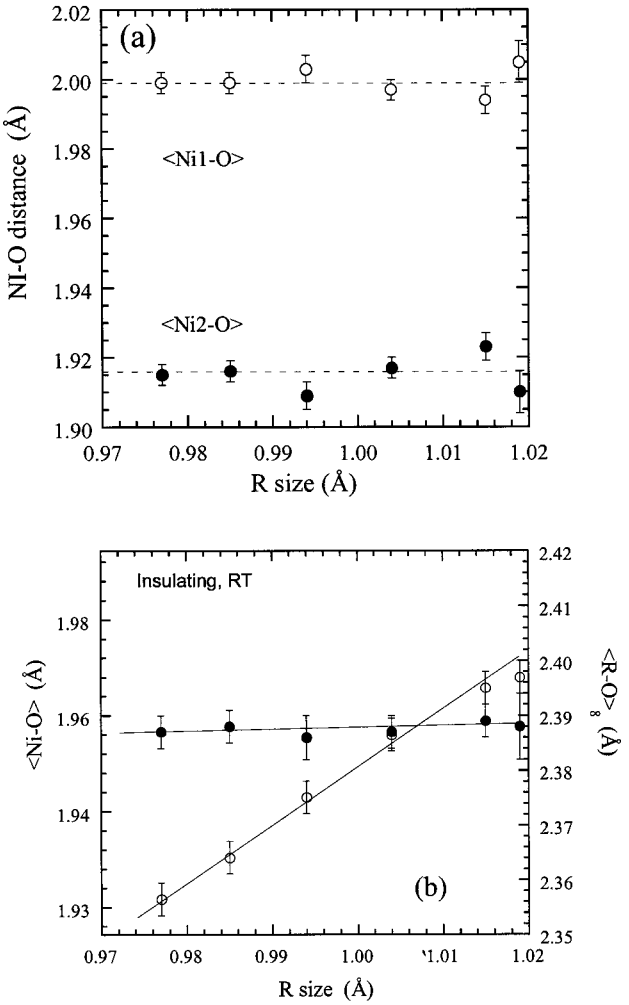

FIG. 5. (a) Evolution of the average Ni1-O and Ni2-O distances in NiO_6 octahedra and (b) average $\langle$Ni-O$\rangle$ and $\langle R\text{-O}\rangle_8$ distances as a function of the R^{3+} ionic radius, at RT in monoclinic RNiO$_3$.

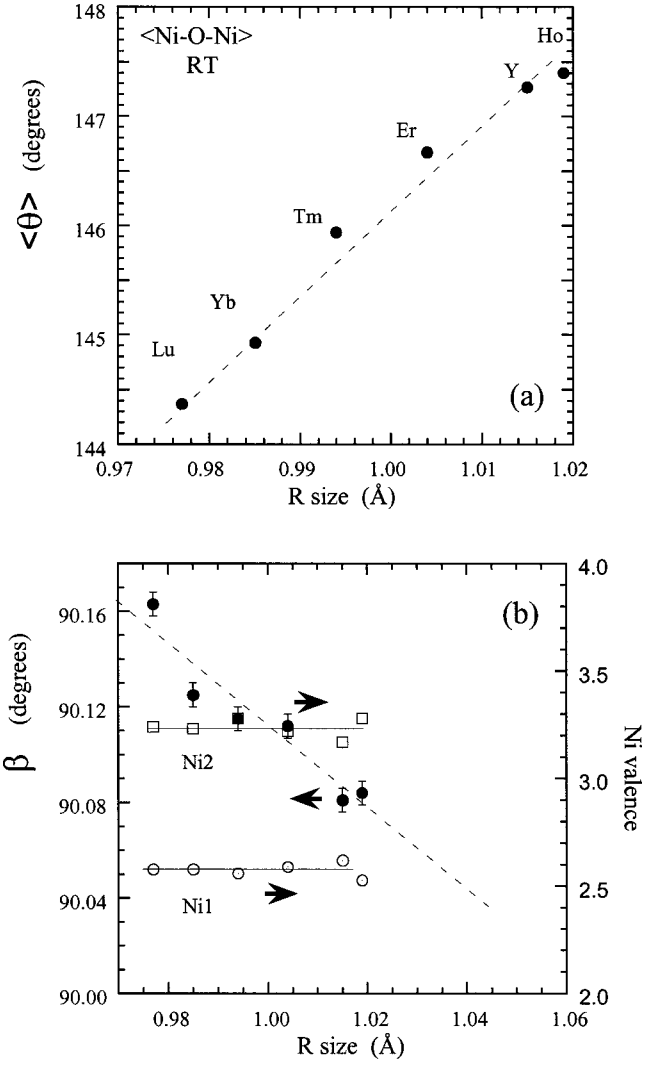

FIG. 6. Dependence of the measured $\theta=\langle$Ni-O-Ni$\rangle$ bond angle, and (b) the evolution of the monoclinic angle β and Ni valences with R^{3+} size.

tropic peak broadening.[12] In the monoclinic perovskites there is no evidence of such structural faults, and their diffraction peaks are much narrower. In this direction it is useful to verify that the GII, which gives an idea of the structural strain, does not significantly evolve along the series. This is shown in Table III. Therefore, the symmetry reduction from orthorhombic to monoclinic, with the concomitant increase of positional degrees of freedom, enables the relaxation of such strain.

According to the present results, even if a macroscopic deviation of β from 90° has not been detected in the early rare-earth nickelates, the same charge segregation phenomena with a value of δ_{eff} not very different from 0.3 could very likely be present in the insulating regime of the less-distorted oxides. Taking into consideration the remarkable pseudocubic character of the lattice observed in the former members of the RNiO$_3$ series, and that orbital ordering or cooperative arrangement of JT distorted octahedra is precluded, or at least minimized in these materials, the observation of an external manifestation of the charge disproportionation phenomena in the lighter rare-earth nickelates remains a difficult task.

CONCLUSIONS

We have shown that the monoclinic structure first observed in $YNiO_3$ and $HoNiO_3$, at the opening of the gap below T_{MI}, is a common feature in the insulating regime of the last members of the RNiO$_3$ perovskites (for the smaller R^{3+} cations). The insulating phase of these nickelates with enhanced electron-lattice coupling consists of expanded ($Ni1O_6$) and contracted ($Ni2O_6$) octahedra that alternate along the three directions of the crystal. These results show evidence of the stabilization of an uncompleted charge disproportionation, $2Ni^{3+} \rightarrow Ni^{3+\delta} + Ni^{3-\delta}$. The mean charge modulation between Ni1 and Ni2 sites is about $2\delta = 0.6$ electrons, and does not significantly evolve along the series. It appears to be independent of the distortion degree of the perovskite, characterized by the θ tilting angle of the NiO_6 octahedra, and the parameter β quantifying the deviation from the orthorhombic cell. This result is relevant because it suggests that the early members of the RNiO$_3$ series may

undergo the same charge disproportionation phenomenon below T_{MI} even if a significant departure from the orthorhombic symmetry has not been previously detected. The stabilization of a charge-density wave below a characteristic temperature (T_{MI}) could be the universal driving force for the gap opening in the whole family of rare-earth nickelates.

ACKNOWLEDGMENTS

The authors would like to thank the ILL for making available the beam time, and financial support by the OCYT-CYCyT (Project Nos. MAT97-0699, PB97-1181, PB97-1175).

*To whom correspondence should be addressed. Electronic address: ja.alonso@icmm.csic.es

[1] M. Medarde, J. Phys.: Condens. Matter **9**, 1679 (1997).
[2] P. Lacorre, J. B. Torrance, J. Pannetier, A. I. Nazzal, P. W. Wang, and T. C. Huang, J. Solid State Chem. **91**, 225 (1991).
[3] J. B. Torrance, P. Lacorre, A. I. Nazzal, E. J. Ansaldo, and Ch. Niedermayer, Phys. Rev. B **45**, 8209 (1992).
[4] J. L. García-Muñoz J. Rodríguez-Carvajal, P. Lacorre, and J. B. Torrance, Phys. Rev. B **46**, 4414 (1992).
[5] J. B. Goodenough and P. Raccah, J. Appl. Phys. **36**, 1031 (1965).
[6] N. E. Massa, J. A. Alonso, and M. J. Martínez-Lope, Phys. Rev. B **56**, 986 (1997).
[7] M. Medarde, P. Lacorre, K. Conder, F. Fauth, and A. Furrer, Phys. Rev. Lett. **80**, 2397 (1998).
[8] J. M. de Teresa, M. R. Ibarra, P. A. Algarabel, C. Ritter, C. Marquina, J. Blasco, J. García, A. del Moral, and Z. Arnold, Nature (London) **386**, 256 (1997).
[9] J. Rodríguez-Carvajal, M. Hennion, F. Moussa, A. F. Moudden, L. Pinsard, and A. Revcolevschi, Phys. Rev. B **57**, R3189 (1998).
[10] G. Démazeau, A. Marbeuf, P. Pouchard, and P. Hagenmuller, J. Solid State Chem. **3**, 582 (1971).
[11] J. A. Alonso, J. L. García-Muñoz, M. T. Fernández-Díaz, M. A. G. Aranda, M. J. Martínez-Lope, and M. T. Casais, Phys. Rev. Lett. **82**, 3871 (1999).
[12] J. A. Alonso, M. J. Martínez-Lope, M. T. Casais, M. A. G. Aranda, and M. T. Fernández, J. Am. Chem. Soc. **121**, 4754 (1999).
[13] J. Rodríguez-Carvajal, Physica B **192**, 55 (1993).
[14] I. D. Brown, in *Structure and Bonding in Crystals*, edited by M. O'Keeffe and A. Navrotsky (Academic Press, New York, 1981), Vol. 2, pp. 1–30.
[15] N. E. Brese and M. O'Keeffe, Acta Crystallogr., Sect. B: Struct. Sci. **47**, 192 (1991).
[16] I. D. Brown, Z. Kristallogr. **199**, 255 (1992).
[17] J. A. Alonso (unpublished).
[18] J. L. García-Muñoz, M. Suaiidi, M. J. Martínez-Lope, and J. A. Alonso, Phys. Rev. B **52**, 13 563 (1995).
[19] J. Rodríguez-Carvajal, S. Rosenkranz, M. Medarde, P. Lacorre, M. T. Fernández-Díaz, F. Fauth, and V. Trounov, Phys. Rev. B **57**, 456 (1998).
[20] P. G. Radaelli, D. E. Cox, M. Marezio, and S. W. Cheong, Phys. Rev. B **55**, 3015 (1997).
[21] J. B. Goodenough, Phys. Rev. **164**, 785 (1967).
[22] J. L. García-Muñoz, J. Fontcuberta, B. Martínez, A. Seffar, S. Piñol, and X. Obradors, Phys. Rev. B **55**, R668 (1997).
[23] J. A. Alonso, M. J. Martínez-Lope, M. T. Casais, J. L. Martínez, G. Demazeau, A. Largeteau, J. L. García-Muñoz, A. Muñoz, and M. T. Fernández-Díaz, Chem. Mater. **11**, 2463 (1999).